Journal of Nuclear Materials 399 (2010) 175–180

Contents lists available at ScienceDirect

Journal of Nuclear Materials

journal homepage: www.elsevier.com/locate/jnucmat

# Molecular dynamic simulation of fission fragment induced thermal spikes in $UO_2$: Sputtering and bubble re-solution

M. Huang, D. Schwen *, R.S. Averback

*Department of Materials Science and Engineering, University of Illinois at Urbana-Champaign, IL 61801, USA*

ARTICLE INFO

*Article history:*
Received 4 August 2009
Accepted 23 January 2010

ABSTRACT

Sputtering and the re-solution of Xe fission gas bubbles in $UO_2$ due to electronic energy deposition of fission fragments is investigated using molecular dynamic (MD) simulations. First, a two-temperature model coupling the electronic (e-) and phonon (p-) systems is employed to determine the temperature profile along the tracks of fission fragments. The e–p coupling constant within the model is determined by comparing the sputtering yields deduced from the MD simulations with those obtained experimentally. Next, fission fragments tracks are simulated in $UO_2$ containing Xenon bubbles. At high $(dE/dx)_e$ bubbles are partially dissolved, however, for ions with electronic stopping powers lower than 34 keV/nm, no bubble re-solution is observed. Thus, bubble re-solution due to the electronic stopping of fission fragments in $UO_2$ is expected to be insignificant compared to homogeneous re-solution.



## 1. Introduction

With the development of generation IV reactor technology, the impact of intragranular fission gas on the performance of $UO_2$ fuels has gained considerable concern. Gaseous fission fragments (Xe, Kr, etc.) and their precipitation (fission gas bubbles), transport, and segregation are known to adversely influence the thermal and mechanical properties of fuels. Release of these gaseous atoms from bubbles to fuels, moreover, can lead to cladding failure at high burn-ups. In view of these deleterious effects of fission gas in fuels, predicting the evolution of the size and population of fission gas bubbles is crucial in determining fuel performance in future reactors.

The available analytical models for calculating bubble populations have been discussed in a recent review paper by Olander and Wongsawaeng [1]. These models consider two mechanisms for the re-solution of gas atoms from bubbles. The first, homogeneous re-solution, describes the interaction of the fission fragments with fission gas bubbles through energetic collision cascades. In this case, fission gas atoms are ejected from bubbles by individual binary collision recoil events. In a recent paper [2] we calculated the bubble re-solution histograms for the homogeneous re-solution mechanism based on nuclear stopping using a combination of Monte Carlo (MC) and molecular dynamics (MD) simulations. In our model system of $UO_2$, consisting of Xenon bubbles having a radius of 1 nm and number density of $7 \times 10^{23}$ m$^{-3}$, we found that five Xenon atoms are re-solved on average per bubble per fission fragment [2].

The focus of this work is the local heating arising from the electronic energy loss of the fission fragments, and whether it can cause heterogeneous Xe bubble re-solution. Heterogeneous re-solution describes an unspecified interaction of fission fragments with fission gas bubbles, leading to the instantaneous total or partial re-solution of the contained fission gas into the $UO_2$ matrix. Typical electronic energy losses $(dE/dx)_e$ are ~18 keV/nm for heavy fission fragments and ~22 keV/nm for light fission fragments [3]. These energetic ions first deposit their energy in the electronic system, heating the electrons; part of the energy is then transferred from hot electrons to the lattice through electron–phonon coupling. This process produces a cylindrical thermal spike around the ion trajectory. Such a thermal spike could easily reach temperatures above the melting point of the material, and if the spike intersected a gas bubble, a purely thermally-driven re-solution might take place. This re-solution mechanism is fundamentally different from the known homogeneous re-solution, as only negligible momentum transfer takes place between fission fragment and gas atoms. The radial temperature distribution around the track can be calculated using the two-temperature model (TTM), as described in a review paper by Assmann et al. [4] for various metals, and the insulators $SiO_2$ and LiF.

Apart from numerous known macroscopic material properties, such as heat capacities and thermal conductivities of both the electron system and the $UO_2$ lattice, a parameter $\lambda$ quantifying the coupling strength between the two heat baths – electrons and lattice – must be obtained separately. The value of $\lambda$ is crucial for the evolution of the temperature distribution around the fission

* Corresponding author. Tel.: +1 217 244 8678; fax: +1 217 244 2946.
*E-mail addresses:* daniel@schwen.de, dschwen@illinois.edu (D. Schwen).

0022-3115/$ - see front matter © 2010 Elsevier B.V. All rights reserved.
doi:10.1016/j.jnucmat.2010.01.015

fragment trajectory. Ultimately it determines the amount of lattice melting and the re-solution of gas atoms from bubbles, but it can also be linked to directly observable phenomena like track formation and electronic sputtering.

Attempts have been made to determine the free parameter $\lambda$ by fitting calculations of ion track damage using the TTM model to experimental data. For example, by assuming that track damage in $UO_2$ becomes visible in a transmission electron microscope (TEM) only after the spike temperature exceeds the melting temperature, i.e., $T > T_m$, Wiss et al. suggested $\lambda = 6$ nm [3]. In a later paper, Toulemonde et al. revised this previous analysis by assuming visible track damage required spike temperatures equivalent to the sublimation energy. Using this criterion, $\lambda$ is found to be 4 nm [5]. The nature of the track damage in $UO_2$, sources for the TEM contrast, and relationship between the two, however, are not yet well understood, making the track formation criteria somewhat speculative.

In the present paper, we adopt a similar procedure for determining $\lambda$, but we consider sputtering data to avoid the ambiguities involved in both defining track damage and relating spike temperature to track damage. This procedure has several advantages: sputtering yields have been measured experimentally, the results are quantitative, and we are able to perform MD simulations to provide a direct connection to the experiments. The TTM is employed to provide the initial temperature distribution in the sample, using $\lambda$ as a parameter. Once the value of $\lambda$ has been determined by this method, we employ it in additional MD simulations to calculate the re-solution of Xe gas bubbles during irradiation of $UO_2$ with fission fragments. The accuracy of the results of course depends on the reliability of the interatomic potentials, as will be discussed, but beyond the quantitative reliability, the simulations also provide a good qualitative understanding of the mechanisms of gas re-solution.

A two-step approach is thus employed to evaluate heat spikes as a possible re-solution mechanism. First, sputtering simulations are used to determine the electron–phonon coupling constant in the TTM for $UO_2$ by fitting the simulations to experimental data; then, the thermal spikes are simulated as a function of electronic stopping power in samples of $UO_2$ containing Xenon bubbles.

The theoretical modeling process of the electronic sputtering yields has three components which are explained in detail in the following two sections. Their interplay is a key point of this work. The first component is the use of TTM to calculate the lattice heating around the fission fragment trajectories as a function of time and space. The next component is a molecular dynamics (MD) simulation of a $UO_2$ surface region. It uses the temperature profile obtained from the TTM as the starting conditions at a time when most of the electronic excitations in the track have converted to lattice heating. This time is so short that no significant amount of sputtering could have occurred earlier. Lastly, a comparison of MD sputtering yields with the experimental sputtering data, using different values of $\lambda$ in the TTM, yields an *effective* $\lambda$ value with which we can exactly reproduce the experimental data in the MD simulations.

## 2. Analytical model

### 2.1. Two-temperature model (TTM)

A model describing thermal spikes induced by swift ions was revised by Toulemonde et al. [6] to explain the appearance of latent tracks induced in materials by the slowing down of ions in the electronic stopping power regime. In this model, the incident ion first deposits its energy into the electron subsystem on a time scale of $\sim 10^{-16}$–$10^{-14}$ s [4]. The electrons then transfer energy to the atoms through electron–phonon coupling, which occurs over a timescale of $\sim 10^{-14}$–$10^{-11}$ s [4]. This process produces a cylindrical region around the trajectory of the energetic ion, where the temperature can often surpass the melting point, $T_m$, of the material.

The TTM describes the temperature evolution of the electronic and atomic subsystems by two coupled differential heat transfer equations in cylindrical geometry [6]:

$$C_e(T_e)\frac{\partial T_e}{\partial t} = \frac{1}{r}\frac{\partial}{\partial r}\left|rK_e(T_e)\frac{\partial T_e}{\partial r}\right| - (T_e - T_a)\cdot g + A(r,t) \quad (1)$$

$$C_a(T_a)\frac{\partial T_a}{\partial t} = \frac{1}{r}\frac{\partial}{\partial r}\left|rK_a(T_a)\frac{\partial T_a}{\partial r}\right| + (T_e - T_a)\cdot g \quad (2)$$

where $T$, $C$, and $K$ are temperature, specific heat coefficient and thermal conductivity of the electrons (index $e$) and atoms (index $a$). These equations are non-linear since $C$ and $K$ are temperature dependent. According to Baranov et al. [7], hot electrons in the conduction band of an insulator are expected to behave like hot electrons in metal. The hot electron specific heat $C_e$ and the hot electron diffusivity $D_e = K_e/C_e$ are thus considered as constants in this model: $C_e \sim 10^6$ J m$^{-3}$ K and $D_e \sim 2\times 10^{-4}$ m$^2$ s$^{-1}$ [8]. The thermodynamic parameters of $UO_2$, such as thermal conductivity, specific heat, density can be found in the literature [3].

The source term $A(r,t)$ describes the energy distribution created by an incident fission fragment in the electronic subsystem. It consists of a Gaussian distribution in time and a radial distribution $F(r)$ of the delta electrons in space, which are obtained from Katz's delta-ray theory [9]:

$$A(r,t) = b\cdot\left(\frac{dE}{dx}\right)_e\cdot\exp\left(-\frac{(t-t_0)^2}{2t_0^2}\right)\cdot F(r) \quad (3)$$

Here, $t_0$ represents the time for the electrons to thermally equilibrate ($\sim 4\times 10^{-15}$ s) [4]. The factor $b$ ensures that the integration of $A(r,t)$ in space and time is equal to the total electronic stopping power $(dE/dx)_e$.

$$\int_0^\infty dt\int_0^\infty A(r,t)\cdot 2\pi r dr = \left(\frac{dE}{dx}\right)_e \quad (4)$$

The energy transfer from electrons to atoms is represented by the product of the coupling constant $g$ and the temperature difference $(T_e - T_a)$. When the electrons cool below the lattice temperature, they are assumed to be trapped in the lattice, and hence the e–p coupling is suppressed [4]. In our calculations, we reset $g$ to zero to turn off the electron–phonon coupling when $T_e < T_a$. For insulators, the electron–phonon coupling constant $g$ is generally expressed in terms of the parameter $\lambda$, a mean diffusion length for the energy in the coupled system, through the relation $\lambda^2 = C_e\cdot D_e/g$. In the TTM calculations, a small value for $\lambda$ will yield a high lattice temperature at the center of the spike. This is a consequence of the larger difference in temperature in the electron and phonon systems and the longer time available for the electrons to transfer energy to the lattice before diffusing radially outward.

It should be noted that in our simulation we neglect radiation losses at the free surface. While the electron temperatures reach up to $10^5$ K these excitations last for only $\approx 10^{-13}$ s, and despite the $T^4$ dependence in the Stefan–Boltzmann law this amounts only to 1% of the energy deposited into the first unit cell layer, even when assuming an emissivity of one. Cooling by evaporation is similarly negligible,

### 2.2. Sputtering yield

Before reporting the results of the MD simulations, we calculate sputtering yields using the Sigmund thermal spike model [10]. This will be useful later for scaling our MD results. In the Sigmund mod-

el, the evaporation flux $\Phi(T_a(r,t))$ is given as a function of the lattice temperature at the surface, $T_a(r,t)$:

$$\Phi(T_a(r,t)) = N\sqrt{\frac{kT_a(r,t)}{2\pi M}}\exp\left(-\frac{U}{kT_a(r,t)}\right), \quad (5)$$

where $N$ is the atomic density, $M$ is the molecular mass of the target, and $U$ is the sublimation energy per sputtered molecule, which is assumed equal to the surface binding energy [4]. $T_a(r,t)$ is obtained using the TTM. The total sputtering yield $Y_{\text{tot}}$ is obtained from the integral of $\Phi(T_a(r,t))$ over time and space:

$$Y_{\text{tot}} = \int_0^\infty dt \int_0^\infty \Phi(T_a(r,t)) \cdot 2\pi r dr \quad (6)$$

Note that this model assumes evaporation from a planar surface and the temperature is taken from a bulk calculation. Furthermore, the model neglects sputtering of clusters larger than a single formula unit and the possible formation of craters.

## 3. MD simulations

### 3.1. Interatomic potential

The MD simulations were performed using LAMMPS [11], which employs the Particle–Particle Particle-Mesh (PPPM) method for treating the long-ranged coulomb interactions between the oxygen and uranium atoms. The non-coulombic pair interactions and their first derivatives were tabulated with a smooth cut-off up to 1.04 nm. The large simulation cells required in this work dictated the choice of a simple rigid-ion potential over a more complex core–shell potential. For the U–U, U–O, and O–O interactions we used the Morelon potential [12] which is described in a recent review of $UO_2$ potentials by Govers et al. [13]. The Xe–U potential has the form of Born–Meyer potentials, while the Xe–Xe and Xe–O interactions are modeled using Lennard–Jones potentials; the parameterization for all three interactions is taken from a recent work by Geng et al. [14]. All interactions are splined to the universal ZBL potential at short ranges. We tested these interactions by calculating the variation of cohesive energy of a sparse $UO_2$ Xe cell as a function of its lattice parameter in MD simulations; our model showed good agreement with the *ab initio* result published in Ref. [14].

The Morelon potential reproduces the lattice parameter across a broad temperature range. While it underestimates the heat capacity by about a factor of two, among comparable potentials, it comes closest to the experimental data. For sputtering calculations, the sublimation energy is a key quantity. Our MD test shows that the Morelon potential yields a sublimation energy of 818.7 kJ/mol for $UO_2$, which is somewhat higher than the experimental value of 616.4 kJ/mol [3]. With this value for the sublimation energy a higher thermal spike peak temperature in MD simulations is needed to obtain the same sputtering yields as the experimental data. Hence a smaller value of $\lambda$ in the TTM calculation, to intensify e–p coupling, will be deduced from our fitting procedure. This will be clarified in what follows.

### 3.2. Sputtering simulations

Simulations of sputtering were performed on samples with (1 1 0) surface planes; these are the lowest index charge neutral planes in the $UO_2$ structure. This choice thus avoids excessive surface relaxation due to the fixed charge potential used in the simulations. A large computational box with periodic boundary conditions and dimensions of about 45 nm × 60 nm × 60 nm was filled with a crystal slab with the dimensions of about 15 nm × 60 nm × 60 nm (4,199,040 atoms), resulting in a sample with two free surfaces. One surface was left unconstrained to allow sputtering. The atoms in the outermost two atomic layers of the other surface were constrained to move only perpendicular to the axis of the spike simulating a semi-infinite crystal below and preventing sputtering. The total thickness of the sample in the direction of the spike was chosen based on several trial simulations. These showed that the sputtering yield becomes independent of the sample thickness for thicknesses greater than 15 nm. Atoms were counted as sputtered as soon as they passed a threshold distance from the original sample surface and were not connected to the bulk by a chain of chemical bonds. This enables reliable detection of sputtered atoms, molecules and larger clusters. Two atomic layers at the periodic boundaries of the sample were maintained at 300 K to approximate heat dissipation to a semi-infinite medium. The thermal spikes were initiated as sets of heated coaxial cylindrical shells along the $x$-direction, as next described.

Our TTM calculations show that the heat transfer from the electronic system to the lattice in $UO_2$ occurs on a timescale of $10^{-14}$–$10^{-13}$ s, and therefore before the onset of any possible phase transitions. The initial radial temperature profile to be used in the MD simulations could therefore be calculated using the TTM without taking into account the enthalpies of fusion and vaporization. We initialized the temperature profile in MD simulation by creating several coaxial cylindrical shells in the sample (along the $x$-axis) with increasing radius, and rescaling the atomic velocities in each shell. Although this produces a discontinuous step-shaped temperature profile as the starting condition, running this initial state for approximately one 1 ps under constant volume and energy (NVE) conditions partitions the energy with other degrees of freedom and smoothes the temperature profile, yielding a temperature distribution in the $UO_2$ system similar to the TTM calculation. Several tests were made to ensure that the thermal spike temperature profile obtained at the end of NVE stage did indeed agree with the TTM calculation. No sputtering is observed during this relaxation phase. Following this initial relaxation period, the $UO_2$ sample was evolved at constant pressure for about 20 ps, after which the sputter yield no longer changed.

### 3.3. Bubble re-solution simulations

Simulations of Xe bubble re-solution were performed using a $UO_2$ sample with a size of 20 × 80 × 80 lattice units with a lattice parameter of 0.546 nm. A single spherical void was incorporated in the $UO_2$ lattice by stoichiometrically removing U and O atoms, thus preserving the overall charge neutrality of the system. The void was subsequently filled with a close-packed Xe lattice, and the system was relaxed at 300 K for ~100 ps. The density of Xe in the relaxed bubble was $\approx 4.2 \times 10^3$ kg/m$^3$ which is in agreement with experimental observations of bubbles of similar size [1]. The resulting Xe bubbles remained compact and spherical during this time, relaxing to a diameter of 2 nm, and without loss of Xe atoms from the bubble. The thermal spike temperatures were then initialized using the same procedure described for the sputtering simulations. The distance of the spike axis from the center of the bubble was varied from 0 nm (spike axis through the center of the bubble) to 1 nm (spike axis tangential with the surface of the bubble). After equilibrating for ≈1 ps under NVE conditions, the sample was allowed to evolve for ≈20 ps under a small constant pressure (NPH) of 0.2 GPa, with a fixed boundary temperature of 300 K.

## 4. Results and discussion

### 4.1. Sputtering

Schlutig [15] measured the sputtering yields of $UO_2$ for several different ions and energies. By comparing these experimental data

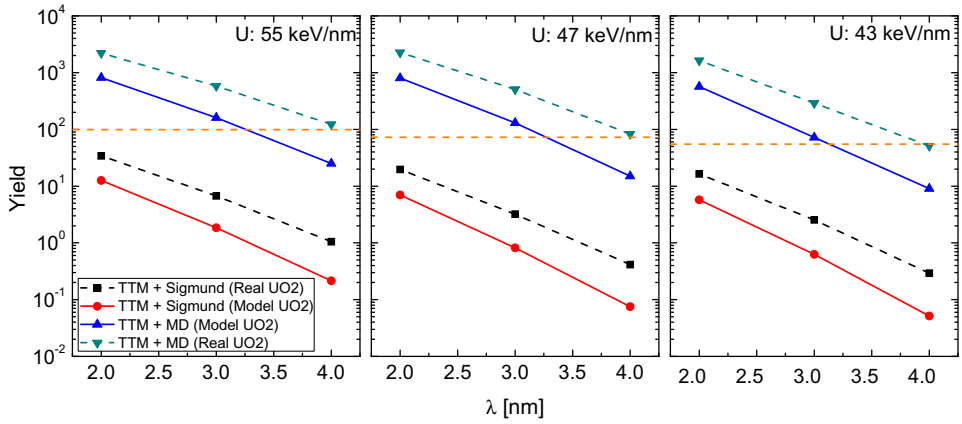


**Fig. 1.** Sputtering yields obtained from MD simulations and Sigmund model calculations plotted as a function of the electron–phonon coupling constant in $\lambda$ in the two-temperature model. The red lines (● symbols) represent Sigmund model with cohesive energy of $UO_2$ from Morelon potential, *X* eV [12]; black lines (■) Sigmund model with actual cohesive energy of $UO_2$, *Y* eV; blue line (?) MD simulation model with Morelon potential, showing agreement with experimental data for $\lambda = 3.2$ nm; green line (▼) MD yield scaled by the ratio of the Sigmund model yields (see text), showing agreement with the experimental data for $\lambda = 4$ nm.

with our sputtering simulation results, we determine the free parameter $\lambda$ for our model of $UO_2$. We chose four stopping powers for the sputtering simulations: $dE/dx$ = 55.4 keV/nm, 47.0 keV/nm, 43.0 keV/nm, and 32.8 keV/nm. The sputtering results (blue[1] line) are shown in Fig. 1 as a function of $\lambda$. By comparing the simulation and experimental sets of data in Fig. 2, using only the three highest stopping powers, we deduce a value of $\lambda = 3.2$ nm for our model $UO_2$ described by the Morelon potential. This value is smaller than the published estimate of $\lambda = 4$ nm [5]. Our smaller value of $\lambda$ is expected since higher thermal spike temperatures are needed to compensate for the higher sublimation energy of our model for $UO_2$ (818.7 kJ/mol), as compared to the experimental value of 616.4 kJ/mol. We now use the Sigmund model of thermal spike sputtering to illustrate this point.

Fig. 1 shows the sputtering yields obtained using the Sigmund model as given by Eq. (6) for each $\lambda$ (the red solid lines). A sublimation energy of 818.7 kJ/mol was assumed in this model, i.e., the value given by the Morelon potential. Notably, the calculated sputtering yields are 2 orders of magnitude lower than the MD results. A similar discrepancy between Eq. (6) and MD simulations was reported in previous published results for other materials [4,16]. The trend in sputtering yields as a function of $\lambda$, however, is well reproduced.

We next changed the sublimation energy in the TTM/Sigmund model from 818.7 kJ/mol to 616.4 kJ/mol, to obtain the analytical sputtering yields for real $UO_2$ (black dash lines in Fig. 2). As expected, the decreased sublimation energy results in higher sputtering yields. By scaling the MD results for our model $UO_2$, using the ratio of these two analytical yields, we obtain the green dashed line, which we assume approximates the sputtering yields for real $UO_2$ in MD. Comparison of these corrected values with the experimental data for $UO_2$ then yields $\lambda = 4.0$ nm. This result now agrees very well with the value of $\lambda$ suggested in previous work [5]. This exercise illustrates two important facts: that for a very reasonable value of $\lambda$, (i) the experimental sputtering yields can be reproduced by our MD model and (ii) sputtering from swift ions can be explained entirely by thermal spike behavior, no other mechanism need be invoked.

One detail in the experiments that the MD model fails to reproduce is the gradual decrease in sputtering yields at electronic stopping powers, below ≈32.8 keV/nm, see Fig. 2. The Sigmund model calculations also fail to show this gradual decrease. We can presently only speculate about the cause of this discrepancy, but we attribute it to the different surface structures employed in the experiment as compared to the MD simulations. The polycrystalline $UO_2$ samples used in the experiment are likely to contain some fraction of high sputter yield surface orientations, defects, and possibly a non-stoichiometric surface layer. At low energies, these effects are likely to result in a base-line sputter yield which changes slowly with the thermal spike energy. At high energies, however, the surface structure becomes less significant as more of the sputtered atoms come from sub-surface regions of the sample and cratering starts to occur.

Finally we comment on the implicit assumption used in scaling our MD data according to the Sigmund model, viz. that the emission of sputtered atoms is a consequence of independent sublimation events and that collective behavior is not important. As a simple check, we analyzed the cluster-size distribution of sputtered atoms in our various MD runs. Clusters larger than four formula units represent only ~15% of the total sputtering yield for any of the simulated stopping powers with $\lambda = 3$ nm, and 0% with $\lambda = 4$ nm (recall that the correct value of $\lambda$ is 3.2 nm). The majority of the sputtered clusters are thus single $UO_2$ molecules.

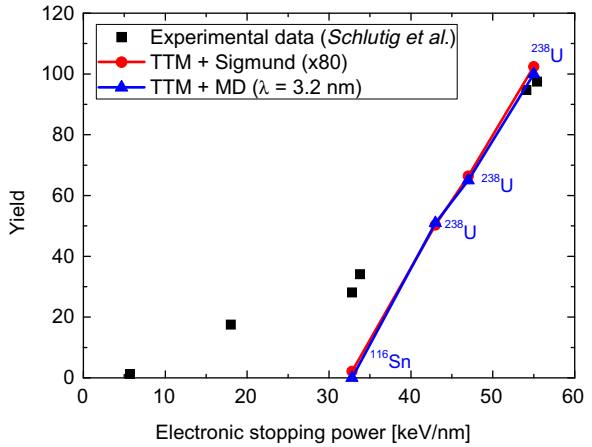


**Fig. 2.** Experimental data of electronic sputtering yields in $UO_2$ as a function of electronic stopping power (■) (from Ref. [15]); sputtering yields from MD simulations based on two-temperature model with $\lambda = 3.2$ nm (?); and sputtering yields from Sigmund model (●) scaled by a factor of 80.

[1] For interpretation of color in Figs. 1–3, the reader is referred to the web version of this article.

**Table 1**
Number (and percentages) of re-solved Xenon atoms from bubbles containing 79 Xenon atoms. Results are given for different electronic stopping power values and two different thermal spike positions, through the center of the bubbles and tangentially along the surface of the bubbles. Each data point is averaged from two MD runs.

| Se (keV/nm) | No. of re-solved Xe atoms | |
|---|---|---|
| | Center | Tangentially |
| 55.4 | 11.5 (14.6%) | 9.5 (12.0%) |
| 47.0 | 5 (6.3%) | 2.5 (3.2%) |
| 32.8 | 0 (0%) | 0 (0%) |

### 4.2. Bubble re-solution

MD simulation of bubble re-solution was calculated in $UO_2$ using the value, $\lambda = 3.2$ nm, which gave the best agreement between the experimental data and the MD sputtering yields using the Morelon potential. For each stopping power, two geometries were considered: (1) the axis of the thermal spike cylinder passing through the center of the bubble (center) and (2) the axis of thermal spike passing tangentially along the outer bubble radius (tangentially). Two events for each condition were run. The results are compiled in Table 1. The main results are that (i) Xe can indeed be re-solved in the matrix due to the thermal spike and (ii) the number of Xe atoms re-solved increases with increasing electronic stopping power. The number of re-solved gas atoms, moreover, is somewhat smaller for the center of the thermal at the bubble periphery than passing through the center. For the lowest fission fragment energy tested, 32.8 keV/nm, no re-solution is observed in either geometry. Thus, no Xe atom re-solution can be expected for fission fragments, regardless of the distance between trajectory of the fission fragment and the bubble center, since the electronic stopping powers of fission fragments do not exceed ≈22 keV/nm in $UO_2$ [3]. We will return to this important point, below.

Fig. 3 shows cross sectional slices through the computational cell during the late stages of the thermal spike, $t \approx 100$ ps. Most of the $UO_2$ lattice (uranium plotted as medium sized red spheres, oxygen as small blue spheres) has recrystallized. The re-solved Xenon atoms (large green spheres) are frozen at their respective positions. As shown in Fig. 4, all movement of re-solved Xenon atoms takes place within the first 30 ps of initiating the event. No atoms are displaced farther than the maximum extent of the molten zone. The displacement of the Xenon atoms occurs via diffusion within the molten zone around the ion track. This is expected, of course, since the simulations only considered the thermal spike associated with the fission fragment, not the energetic recoil events.

While the above simulations provide a clear picture of how fission can re-solve due to thermal spikes created by fission fragments, we wish to point out the number of re-solved Xe atoms calculated by our model represents a maximum value. This is be-

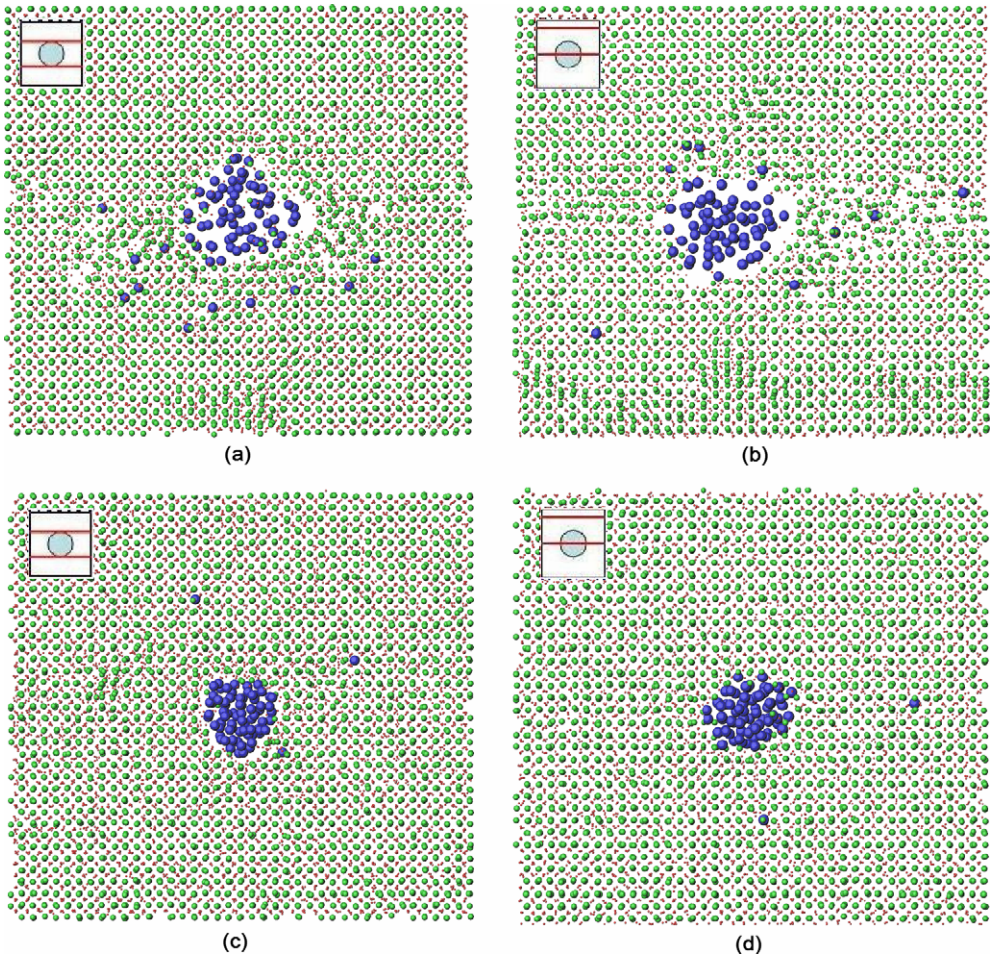


**Fig. 3.** Snapshots of the cross section of $UO_2$ + Xe bubble samples: Xe (large blue spheres), U (medium green spheres), and O (small red spheres). Location of the spike indicated in the inserts. (a) U ion, 55.4 keV/nm, at 116.02 ps, thermal spike axis passing through the bubble center; (b) U ion, 55.4 keV/nm, at 118.84 ps, thermal spike axis is tangent to the bubble surface; (c) U ion: 47.0 keV/nm, at 95.12 ps, the thermal axis passing through the bubble center; (d) U ion, 47.0 keV/nm, at 100.98 ps, thermal spike axis is tangent to the bubble surface. In the high stopping power sample the bubble cavity increases in size and numerous dislocations can be observed around the bubble.

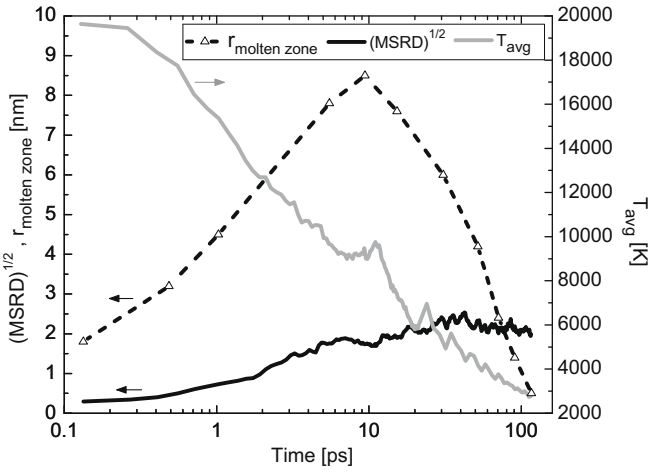


**Fig. 4.** The solid black curve shows the square root of the mean square relative displacement (MSRD) of only the re-solved Xe atoms for the 55.4 keV/nm stopping power case as a function of time. The radius of the molten zone is indicated by the dashed line. The diffusive motion of the re-solved Xe atoms saturates at about 30 ps due to falling temperatures in the periphery of the spike. By 80 ps the re-solved Xe atoms are frozen in the recrystallized matrix. The solid grey line represents the average temperature ($T_{Avg}$) in the center region of the thermal spike ($r < 2.0$ nm).

cause we fixed our value of $\lambda$ using experimental sputtering yields. As we discussed, the effective value of $\lambda$ is lower than what is expected in real $UO_2$, since the sublimation energy deduced from our potential for $UO_2$ is larger than the measured value. We used this value in the simulations of bubble re-solution. Unlike sputtering, however, bubble re-solution should not depend directly on sublimation energy, but rather on a quantity more closely related to the heat of fusion since liquid diffusion is involved. The melting temperature of our potential does reproduce the correct value for real $UO_2$. Consequently, for bubble re-solution, a value closer to $\lambda = 4.0$ nm which we deduced from scaling the sputtering yields for real $UO_2$, might be more appropriate. We performed simulations with that value of $\lambda = 4.0$ as well, and in this case we failed to observe any Xe re-solution for stopping powers less than ≈47 keV/nm. We thus believe our conclusion, that He re-solution induced by thermal spikes is negligible during fission fragment irradiation, is robust and not sensitive to the details of our simulation model.

## 5. Conclusion

We have examined sputtering and bubble dissolution using a hybrid model consisting of a two-temperature model of heat conduction and MD simulation. Comparison of experimental sputtering data with our simulations yielded an electron–phonon coupling constant of $\lambda = 3.2$ nm in the TTM. This value is lower than expected in real $UO_2$, but it is necessary in our model to compensate for the high sublimation energy given by the Morelon potential. Scaling of our results to the correct sublimation energy using the Sigmund model as a guide, however, yields a value of $\lambda = 4.0$ nm, which is the value obtained by other means [5]. Xenon bubble re-solution was then simulated for ions having different electronic stopping powers. Re-solution was observed only for stopping powers greater than ≈35 keV/nm and thus insignificant for fission fragments in $UO_2$, as we next show.

We estimate the maximum rate of Xe re-solution due to fission fragments in $UO_2$. We note that the fall-off of re-solution values as the thermal spike axis shifts from the center to the tangent configuration indicates that the cross section of a fission fragment is no larger than ≈5 nm$^2$. Averaged over the whole decay spectrum, a single fission fragment travels only about 0.5 μm in the fuel matrix while its stopping power exceeds 15 keV/nm. For typical bubble sizes and number-densities, therefore, each fission fragment interacts with ≈1–5 bubbles. Since we calculated that the number of resoluted Xe atoms for a fission fragment in $UO_2$ is zero, the total re-solution rate per fission fragment will also be zero. Even using a value of electronic stopping power = 55.4 keV/nm, which is well over twice the actual value of a fission fragment in $UO_2$, the total re-solution rate is only ≈10–50 Xe atoms per fission fragment. In a previous publication, we showed that the homogeneous re-solution mechanism yields about five re-solved atoms per fission fragment in a similar system. This is only somewhat less than that due to heterogeneous re-solution at the extremely high stopping power. In addition, we never observed total bubble destruction, as assumed in some models of bubble re-solution [17–19]. From these various considerations, we conclude that heterogeneous fission gas re-solution cannot be a significant contribution to bubble evolution in $UO_2$ fuels.

## Acknowledgments

The research was supported by the US Department of Energy, under NERI-C Award No. DE-FG07-14891, and by the US Department of Energy, Basic Energy Sciences under Grant DE-FG02-05ER46217.

## References

[1] D.R. Olander, D. Wongsawaeng, J. Nucl. Mater. 354 (2006) 94.
[2] D. Schwen, M. Huang, R.S. Averback, P. Bellon, J. Nucl. Mater. 392 (2009) 35.
[3] T. Wiss, Hj. Matzke, C. Trautmann, M. Toulemonde, S. Klaumunzer, Nucl. Instrum. Method B 122 (1997) 583.
[4] W. Assmann, M. Toulemonde, C. Trautmann, Topics Appl. Phy. 110 (2007) 401.
[5] M. Toulemonde, Ch. Dufour, A. Meftah, E. Paumier, Nucl. Instr. Meth. Phys. Res. B 166–167 (2000) 903.
[6] M. Toulemonde, E. Paumier, C. Dufour, Radiat. Eff. Defects Solids 126 (1993) 201.
[7] I.A. Baranov, Yu V. Martynenko, S.O. Tsepelevitch, Yu N. Yavlinskii, Sov. Phys. Usp. 31 (1988) 1015.
[8] M. Toulemonde, J.M. Costantini, Ch. Dufour, A. Meftah, E. Paumier, F. Studer, Nucl. Instr. Meth. Phys. Res. B 116 (1996) 37.
[9] M.P.R. Waligorski, R.N. Hamm, R. Katz, Nucl. Tracks Radiat. Meas. 11 (6) (1986) 309.
[10] P. Sigmund, C. Claussen, J. Appl. Phys. 52 (1981) 990.
[11] S.J. Plimpton, Fast parallel algorithms for short-range molecular dynamics, J. Comp. Phys. 117 (1995) 1. http://lammps.sandia.gov.
[12] N.D. Morelon, D. Ghaleb, J.M. Delaye, L.V. Brutzel, Philos. Mag. 83 (2003) 1533.
[13] K. Govers, S. Lemehov, M. Hou, M. Verwerft, J. Nucl. Mater. 376 (2008) 66.
[14] H.Y. Geng, Y. Chen, Y. Kaneta, M. Kinoshita, J. Alloy Compd. 457 (2008) 465–471.
[15] S. Schlutig, Thesis, University of Caen, 2001.
[16] E.M. Bringa, M. Jakas, R.E. Johnson, Nucl. Instr. Meth. Phys. Res. B 164–165 (2000) 762.
[17] H. Blank, Hj. Matzke, Radiat. Eff. 17 (1953) 17.
[18] R. Whapham, Nucl. Appl. 2 (1966) 123–130.
[19] J.A. Turnbull, J. Nucl. Mater. 38 (1971) 203–212.